NRC Research Press

ARTICLE

Photoabsorption spectra from time-dependent auxiliary density functional theory

Javier Carmona-Espíndola and Andreas M. Köster

Abstract: Time-dependent auxiliary density perturbation theory (TDADPT) is extended to the calculation of excited states. The resulting time-dependent auxiliary density functional theory (TDADFT) is structurally identical to the original formulation of Casida. However, significant simplifications occur for the Coulomb and exchange–correlation response due to the underlying auxiliary density functional theory. Here, we present the working equations for TDADFT and a new implementation. Because this new parallel TDADFT implementation is particularly well suited for the calculation of large numbers of excitations, we validate it by the calculation of photoabsorption spectra. Direct comparison with experiment underlines the accuracy and reliability of TDADFT. For selected peaks of the studied polycyclic aromatic hydrocarbon spectra, the assignments of the underlying excitations are also presented.

Key words: photoabsorption spectra, polycyclic aromatic hydrocarbons, time-dependent auxiliary density functional theory, perturbation theory.

Résumé : On étend la théorie de la perturbation de la fonctionnelle de la densité auxiliaire dépendantes du temps (TDADPT) au calcul des états excités. La théorie de la fonctionnelle de la densité auxiliaire dépendante du temps (TDADFT) résultante est structurellement identique à la formulation originale de Casida. Cependant, la théorie de la fonctionnelle de la densité auxiliaire sous-jacente donne lieu à des simplifications importantes de la réponse coulombienne et d'échange-corrélation. On présente ici les équations de travail pour la TDADFT ainsi qu'une nouvelle mise en œuvre. Comme cette nouvelle mise en œuvre parallèle de la TDADFT convient particulièrement bien pour le calcul de grands nombres d'excitations, on la valide par le calcul des spectres de photoabsorption. Une comparaison directe avec l'expérience met en relief l'exactitude et la fiabilité de la TDADFT. On présente aussi l'attribution des excitations sous-jacentes pour certains pics des spectres des hydrocarbures aromatiques polycycliques étudiés. [Traduit par la Rédaction]

Mots-clés : spectres de photoabsorption, hydrocarbures aromatiques polycycliques, théorie de la fonctionnelle de la densité auxiliaire dépendante du temps, théorie des perturbations.

Introduction

Time-dependent density functional theory (TDDFT) is the generalization of ground state density functional theory (DFT) to time-dependent phenomena.[1–12] In most practical applications, TDDFT is employed to describe the interaction between molecules and time-dependent electromagnetic fields. The Runge–Gross theorem represents the time-dependent analogue to the first Hohenberg–Kohn theorem and constitutes the cornerstone of the formal foundation of the time-dependent Kohn–Sham formalism.[8]

Real-time TDDFT has been intensively used for the calculation of photoabsorption spectra of organic molecules,[13–15] clusters,[13,16,17] and biomolecules.[18] For the calculation of photoabsorption spectra, this technique is based on the interaction of the system with a time-dependent electric field. As a result, occupied molecular orbitals are propagated in time. From the induced density, the time-dependent-induced dipole moment is then extracted for the calculation of the photoabsorption spectra. This technique is very efficient for the calculation of photoabsorption spectra. However, information about the excitations in terms of molecular orbital theory, i.e., which molecular orbitals participate in a given excitation, is lost. This is rather unfortunate because this information is crucial for the photochemical analysis of fluorescence and phosphorescence.

Recently, a new methodology, auxiliary density perturbation theory (ADPT), was presented for the calculation of response properties[19–25] in the framework of auxiliary density functional theory (ADFT).[26,27] One of the main reasons for using ADFT is the dramatic reduction in computational demands without sacrificing the accuracy of the underlying Kohn–Sham formalism. The improved computational efficiency is due to the variational fitting of the Coulomb potential[28–30] and the use of the resulting approximated density for the calculation of the exchange–correlation energy and potential. Because ADFT is variational, analytic derivatives can be formulated. Time-dependent auxiliary density perturbation theory (TDADPT), the extension of ADPT to the frequency domain,[31] has been applied for the calculation of frequency dependent response properties such as dynamic polarizabilities and hyperpolarizabilities.[31–34] In this work, the natural extension of TDADPT to the calculation of excited states is presented. This formulation shows that TDADPT converges to the well-known time-dependent auxiliary density functional theory (TDADFT) approach of Casida.[35–37]

This work presents a new TDADFT implementation in the program deMon2k,[38,39] which is well suited for the calculation of

Received 12 December 2012. Accepted 14 February 2013.

J. Carmona-Espíndola. Departamento de Química, Universidad Autónoma Metropolitana-Iztapalapa Av. San Rafael Atlixco N° 186, Col. Vicentina C.P. 09340, Iztapalapa, México D.F.
A.M. Köster. Departamento de Química, CINVESTAV, Avenida Instituto Politécnico Nacional 2508, A.P. 14-740 México D.F. 07000, México.
Corresponding author: Andreas M. Köster (e-mail: akoster@cinvestav.mx).

This article is dedicated to Prof. Dennis R. Salahub in honour of his career contributions to quantum chemistry.

This article is part of a Special Issue dedicated to Professor Dennis Salahub in recognition of his contributions to theoretical and computational chemistry.

Published at www.nrcresearchpress.com/cjc on 26 February 2013.

large numbers of excited states. The main differences to the previous implementation of TDADFT[37] in deMon2k is the reduction of memory demand for the allocation of the three-center electron repulsion integrals (ERIs) in molecular orbital (MO) representation. In fact, our new algorithm does not require ERIs in MO representation. Besides this algorithmic change, a new matrix–vector multiplication scheme within the Davidson diagonalizer[40,41] and the parallelization of the TDADFT branch ensures high computational efficiency. In particular, the full parallelization of the TDADFT branch in deMon2k allows the calculation of thousands of excitations for small molecules with less than 100 atoms. Therefore, TDADFT can be used to calculate photoabsorption spectra to energies up to 30 eV that were so far only accessible by real time TDDFT simulations.[13,14] The advantage of TDADFT photoabsorption spectra simulation is that information of individual excitations become accessible, i.e., singlet–singlet or singlet–triplet excitations. Because these excitations are calculated as the poles of the dynamic polarizabilities, each excitation contains information about which occupied and unoccupied molecular orbitals participate. Thus, a detailed analysis of photoabsorption spectra in terms of MO transitions becomes available.

To validate our new TDADFT algorithm and to show the computational efficiency of its implementation, we present photoabsorption spectra of polycyclic aromatic hydrocarbons that are also used in astrophysical modelling[42–46] to determine these molecules in outer space. In particular, we present TDADFT photoabsorption spectra of benzene, naphthalene, 2-methylnaphthalene, and anthracene. Because experimental[42,43] and real time TDDFT[14,15] photoabsorption spectra are available for these systems, a direct comparison with our TDADFT results is possible. Furthermore, we use the ability of TDADFT to assign individual excitations to analyze the nature of selected peaks in the spectra of these molecules. To this end, we analyze the molecular orbital transitions that are involved in these peaks. It is also worthwhile to mention that all calculations presented here were performed without any kind of symmetry constraints both in the structure optimizations as well as in the TDADFT calculations.

The paper is organized in the following manner. In the next section, the basic theory and implementation details are presented. The computational methodology is then given. The results are discussed and final conclusions are drawn.

Theory

The basic idea of DFT is to describe a microscopic system through its density and not via its wave function. This idea leads to a remarkable reduction of complexity because the $3N$ spacial degrees of freedom of the wave function, N being the number of electrons, are reduced to 3 degrees of freedom in the density. This dramatic reduction of the spacial dimensionality of the problem permits first-principle DFT calculations on large systems with hundreds or even thousands of atoms.[27,39] At the same time, the accuracy of Kohn–Sham DFT calculations match well with correlated wave function approaches in many instances. This has made Kohn–Sham DFT the method of choice for a large variety of electronic structure calculations on atoms, molecules, and solids. Traditional ground state Kohn–Sham DFT calculations rely on the Hohenberg–Kohn theorems and on the existence of a noninteracting system in such a way that the electronic density of the noninteracting system must match the density of the interacting system.

The Runge–Gross theorem is the extension of the Hohenberg–Kohn theorems to time-dependent systems. It states that for every single particle potential, $v(\mathbf{r},t)$, which can be expanded into a Taylor series with respect to the time coordinate around $t = t_0$, a map, $G: v(\mathbf{r},t) \mapsto \rho(\mathbf{r},t)$, is defined by solving the time-dependent Schrödinger equation with a fixed initial state, $\Psi(\mathbf{r}_0,t_0)$, and calculating the corresponding density, $\rho(\mathbf{r},t)$. This map can be inverted up to an additive merely time-dependent function in the potential. Therefore, the density of a time-dependent system determines the time-dependent potential, which in turn determines the time-dependent wave function, $\Psi(\mathbf{r},t)$, up to a time-dependent phase factor. As a result, the time-dependent wave function is a functional of the time-dependent density. To derive the time-dependent Kohn–Sham equations, a time-dependent noninteracting reference system is postulated. It is connected to the real interacting system by a single-particle potential $v_S(\mathbf{r},t)$ that equals the noninteracting electron density, $\rho_S(\mathbf{r},t)$, with the exact electron density, $\rho(\mathbf{r},t)$, of the real system.[47] The noninteracting system consists of a set of noninteracting electrons, which are described by time-dependent orbitals, $\psi_i(\mathbf{r},t)$. Its density is given by

$$\rho(\mathbf{r},t) \equiv \rho_S(\mathbf{r},t) = \sum_i^N |\psi_i(\mathbf{r},t)|^2 \tag{1}$$

The corresponding time-dependent Kohn–Sham equations then take the form

$$\left(-\frac{1}{2}\nabla^2 + v(\mathbf{r},t) + \int \frac{\rho(\mathbf{r}',t)}{|\mathbf{r}-\mathbf{r}'|}d\mathbf{r}' + v_{xc}[\rho;\mathbf{r},t]\right)\psi_i(\mathbf{r},t) = i\frac{\partial \psi_i(\mathbf{r},t)}{\partial t} \tag{2}$$

Here, the time-dependent exchange–correlation potential is defined as

$$v_{xc}[\rho;\mathbf{r},t] = \frac{\delta A_{xc}[\rho;\mathbf{r},t]}{\delta \rho(\mathbf{r},t)} \tag{3}$$

The exchange–correlation action, $A_{xc}[\rho;\mathbf{r},t]$, is a functional of $\rho(\mathbf{r},t)$ in time and space. To simplify the functional dependency, we now introduce the adiabatic approximation, which represents a local approximation in time very much the same as the local density approximation (LDA) in space. Thus, all variations in time are expressed over the time dependency of the density, whereas the exchange–correlation potential is time independent. As a result, the exchange–correlation potential can be calculated directly from the exchange–correlation energy as

$$v_{xc}[\rho;\mathbf{r}] = \frac{\delta E_{xc}[\rho;\mathbf{r}]}{\delta \rho(\mathbf{r},t)} \tag{4}$$

After the general frame of TDDFT is set, we now turn to the calculation of excited states in the framework of ADFT. To this end, we start our derivation with the first order response of the Kohn–Sham and density matrices. From the first order commutator between the perturbed Kohn–Sham and projector matrix follows[31]

$$[\mathbf{K}, \mathbf{P}^{(\lambda)}(\omega)] + [\mathbf{K}^{(\lambda)}(\omega), \mathbf{P}] = \omega \mathbf{P}^{(\lambda)}(\omega) \tag{5}$$

Note that the here appearing matrices are in molecular orbital representation. Thus, the perturbed Kohn–Sham matrix is given as

$$K_{pq}^{(\lambda)}(\omega) = \Gamma_{pq}^{(\lambda)} + \sum_{\bar{k}} \langle pq\|\bar{k}\rangle \left(x_{\bar{k}}^{(\lambda)}(\omega) + z_{\bar{k}}^{(\lambda)}(\omega)\right) \tag{6}$$

Here, p and q represent molecular orbitals and $\bar{k}$ auxiliary functions. The superscript (λ) denotes the perturbation and ω corre-

sponds to the frequency of the external oscillating electric field. $\Gamma^{(\lambda)}_{pq}$ is a molecular dipole moment integral of the form

$$\Gamma^{(\lambda)}_{pq} = \langle p | r_\lambda q \rangle \tag{7}$$

that arises from external field perturbation. The $x^{(\lambda)}_{\bar{k}}(\omega)$ and $z^{(\lambda)}_{\bar{k}}(\omega)$ are the perturbed Coulomb and exchange–correlation fitting coefficients. As usual, $z^{(\lambda)}_{\bar{k}}(\omega)$ can be reduced to perturbed Coulomb fitting coefficients by[31]

$$z^{(\lambda)}_{\bar{k}}(\omega) = \sum_{\bar{l},\bar{m}} G^{-1}_{\bar{k}\bar{l}} f_{\bar{l}\bar{m}} x^{(\lambda)}_{\bar{m}}(\omega) \tag{8}$$

In eq. [8], **G** and **f** are the Coulomb and exchange–correlation kernel matrices, respectively. The idempotence condition for the first order density matrix in molecular orbital representation is given by the following expression:

$$\mathbf{P}^{(\lambda)}(\omega) = \mathbf{P}\mathbf{P}^{(\lambda)}(\omega) + \mathbf{P}^{(\lambda)}(\omega)\mathbf{P} \tag{9}$$

Expanding eq. [5] yields

$$\sum_q \left(K_{pq}P^{(\lambda)}_{qr}(\omega) - P^{(\lambda)}_{pq}(\omega)K_{qr} + K^{(\lambda)}_{pq}(\omega)P_{qr} - P_{pq}K^{(\lambda)}_{qr}(\omega)\right) = \omega P^{(\lambda)}_{pr}(\omega) \tag{10}$$

Because eq. [9] restricts the form of $\mathbf{P}^{(\lambda)}(\omega)$ in eq. [10] such that occupied–occupied and unoccupied–unoccupied blocks are equal to zero and the only nonzero contributions are occupied–unoccupied and unoccupied–occupied blocks, the following two equations are obtained:

$$\left(K_{ii}P^{(\lambda)}_{ia}(\omega) - P^{(\lambda)}_{ia}(\omega)K_{aa} - P_{ii}K^{(\lambda)}_{ia}(\omega)\right) = \omega P^{(\lambda)}_{ia}(\omega) \tag{11}$$

$$\left(K_{aa}P^{(\lambda)}_{ai}(\omega) - P^{(\lambda)}_{ai}(\omega)K_{ii} + K^{(\lambda)}_{ai}(\omega)P_{ii}\right) = \omega P^{(\lambda)}_{ai}(\omega) \tag{12}$$

As always, *i* and *a* refer to occupied and unoccupied molecular orbitals, respectively. To eliminate the explicit dependency from the density fitting coefficients in the perturbed Kohn–Sham matrix, we employ the following equality:

$$x^{(\lambda)}_{\bar{m}}(\omega) = \sum_{\bar{n}} G^{-1}_{\bar{m}\bar{n}} \sum_{rs} \langle \bar{n} \| rs \rangle P^{(\lambda)}_{rs}(\omega) \tag{13}$$

Inserting eq. [13] into eq. [6] leads to

$$K^{(\lambda)}_{pq}(\omega) = I^{(\lambda)}_{pq} + \sum_{\bar{k}\bar{l}} \sum_{rs} \langle pq | | \bar{k} \rangle G^{-1}_{\bar{k}\bar{l}} \langle \bar{l} | | rs \rangle P^{(\lambda)}_{rs}(\omega) + \sum_{\bar{k}\bar{l}} \sum_{\bar{m}\bar{n}} \sum_{rs} \langle pq | | \bar{k} \rangle G^{-1}_{\bar{k}\bar{l}} \langle \bar{l} | f_{xc} | \bar{m} \rangle G^{-1}_{\bar{m}\bar{n}} \langle \bar{n} | | rs \rangle P^{(\lambda)}_{rs}(\omega) \tag{14}$$

This concludes the new derivation of the basic TDDFT working equations in the framework of ADFT. The form of the molecular orbital perturbed Kohn–Sham matrix permits us to express eqs. [11] and [12] in terms of perturbed molecular orbital density matrices. After rearrangement, these two equation systems can be cast in the following matrix form:

$$\underbrace{\left(\begin{bmatrix} \mathbf{A} & \mathbf{B} \\ \mathbf{B}^* & \mathbf{A}^* \end{bmatrix} - \omega \begin{bmatrix} 1 & 0 \\ 0 & -1 \end{bmatrix}\right)}_{\mathbf{R}} \begin{bmatrix} \mathbf{X} \\ \mathbf{Y} \end{bmatrix} = -\begin{bmatrix} \mathbf{\Gamma} \\ \mathbf{\Gamma}^* \end{bmatrix} \tag{15}$$

The elements of the matrices **A** and **B** are given by

$$A_{ia,jb} = \delta_{ij}\delta_{ab}(\epsilon_a - \epsilon_i) + \sum_{\bar{m},\bar{n}} \langle ia \| \bar{m} \rangle G^{-1}_{\bar{m}\bar{n}} \langle \bar{n} \| jb \rangle + \sum_{\bar{m},\bar{n}} \sum_{\bar{k},\bar{l}} \langle ia \| \bar{k} \rangle G^{-1}_{\bar{k}\bar{l}} \langle \bar{l} | f_{xc} | \bar{m} \rangle G^{-1}_{\bar{m}\bar{n}} \langle \bar{n} \| jb \rangle \tag{16}$$

$$B_{ia,jb} = \sum_{\bar{m},\bar{n}} \langle ia \| \bar{m} \rangle G^{-1}_{\bar{m}\bar{n}} \langle \bar{n} \| bj \rangle + \sum_{\bar{m},\bar{n}} \sum_{\bar{k},\bar{l}} \langle ia \| \bar{k} \rangle G^{-1}_{\bar{k}\bar{l}} \langle \bar{l} | f_{xc} | \bar{m} \rangle G^{-1}_{\bar{m}\bar{n}} \langle \bar{n} \| bj \rangle \tag{17}$$

Here, *i,j* and *a,b* refer to occupied and unoccupied molecular orbitals, respectively. For consistency with the notation in the literature, we introduced the vectors **X** and **Y** defined as

$$X_{ai} = P^{(\lambda)}_{ai}(\omega) \tag{18}$$

and

$$Y_{ai} = P^{(\lambda)}_{ia}(\omega) \tag{19}$$

In the case of a resonant excitation, i.e., at the poles of the dynamic polarizabilities, the elements of the perturbed density matrix tend to infinity. Because the right hand side of eq. [15] is finite at all frequencies, **R** = 0 must hold in the case of resonant excitations. Thus, the following generalized eigenvalue equation for the determination of the resonant excitation frequencies, ω, can be formulated:

$$\begin{bmatrix} \mathbf{A} & \mathbf{B} \\ \mathbf{B}^* & \mathbf{A}^* \end{bmatrix} \begin{bmatrix} \mathbf{X} \\ \mathbf{Y} \end{bmatrix} = \omega \begin{bmatrix} 1 & 0 \\ 0 & -1 \end{bmatrix} \begin{bmatrix} \mathbf{X} \\ \mathbf{Y} \end{bmatrix} \tag{20}$$

The solutions, ω, of this generalized eigenvalue equation represent single electron excitation energies. The corresponding pseudo-eigenvectors, **X** and **Y**, collect the transition densities for these excitations and de-excitations. In this form, the pseudo-eigenvalue eq. [20] resembles the well-known random phase approximation (RPA). It was first derived by Casida[35] in the framework of DFT. One of the main features of the presented derivation is that we are not using a formula for the resolution of the identity.[37] Instead, we are employing the perturbation equations from the variational fitting of the Coulomb and exchange–correlation potential. In the following section, we present a new implementation of the calculation of the single excitations, ω. This implementation is not employing the charge conservation constraint in the auxiliary density. Previous validations of TDADFT[37,48] indicated that the charge conservation constraint yields no improvement for the excitations energies, ω, and the oscillator strengths. The advantages of our new implementation are the reduced memory demand and time requirements for TDADFT calculations.

Equation system

The generalized eigenvalue equation system, eq. [20], yields all single excitations and de-excitations in the system. Thus, it is possible to reduce the dimensionality of the problem by combining excitations with their corresponding de-excitations. In case of real molecular orbitals, we can extract the following two equations from eq. [20]:

$$\mathbf{A}\mathbf{X} + \mathbf{B}\mathbf{Y} = \omega\mathbf{X} \tag{21}$$

and

$$\mathbf{BX} + \mathbf{AY} = -\omega\mathbf{Y} \quad (22)$$

The addition and subtraction of eqs. [21] and [22] yield

$$(\mathbf{A} + \mathbf{B})(\mathbf{X} + \mathbf{Y}) = \omega(\mathbf{X} - \mathbf{Y}) \quad (23)$$

and

$$(\mathbf{A} - \mathbf{B})(\mathbf{X} - \mathbf{Y}) = \omega(\mathbf{X} + \mathbf{Y}) \quad (24)$$

respectively. Inserting eq. [24] into eq. [23] leads to

$$(\mathbf{A} - \mathbf{B})(\mathbf{A} + \mathbf{B})(\mathbf{X} + \mathbf{Y}) = \omega^2(\mathbf{X} + \mathbf{Y}) \quad (25)$$

Now, if (**A** – **B**) is positive definite, eq. [25] can be multiplied from the left hand side by $(\mathbf{A} - \mathbf{B})^{-1/2}$ yielding the following equation system:

$$\mathbf{\Omega F} = \omega^2\mathbf{F} \quad (26)$$

with

$$\mathbf{\Omega} = (\mathbf{A} - \mathbf{B})^{1/2}\ (\mathbf{A} + \mathbf{B})(\mathbf{A} - \mathbf{B})^{1/2} \quad (27)$$

and

$$\mathbf{F} = (\mathbf{A} - \mathbf{B})^{-1/2}\ (\mathbf{X} + \mathbf{Y}) \quad (28)$$

The elements of the matrix $\mathbf{\Omega}$ in eq. [27] are given by

$$\Omega_{ai,bj} = \delta_{ab}\delta_{ij}(\epsilon_a - \epsilon_i)^2 + 2\sqrt{\epsilon_a - \epsilon_i}\ K_{ai,bj}\sqrt{\epsilon_b - \epsilon_j} \quad (29)$$

with

$$K_{ai,bj} = \sum_{\overline{m},\overline{n}} \langle ai\|\overline{m}\rangle G^{-1}_{\overline{m}\overline{n}}\langle\overline{n}\|bj\rangle + \sum_{\overline{m},\overline{n}}\sum_{\overline{k},\overline{l}} \langle ai\|\overline{k}\rangle G^{-1}_{\overline{k}\overline{l}}\langle\overline{l}|f_{xc}|\overline{m}\rangle G^{-1}_{\overline{m}\overline{n}}\langle\overline{n}\|bj\rangle \quad (30)$$

The dimension of the eigenvalue equation, eq. [26], is given by the number of configuration interaction single (CIS) excitations, which is the product of the number of occupied and unoccupied molecular orbitals. For a restricted close shell system, the $\mathbf{\Omega}$ matrix can be split into two separated matrices, $\mathbf{\Omega}^{\mathbf{S}}$ and $\mathbf{\Omega}^{\mathbf{T}}$, to calculate singlet–singlet and singlet–triplet excitation energies.[49–52] However, $\mathbf{\Omega}$ is usually too large for a direct diagonalization. Moreover, not all eigenvalues of $\mathbf{\Omega}$ are of interest. Usually only the most low-lying eigenvalues, ω^2, that correspond to low-lying excited states are of interest. For this reason, a subspace diagonalizer is used to find some solutions of eq. [26]. It is well known that the computational bottleneck in this kind of subspace diagonalizers is the matrix–vector multiplication; in our case, the multiplication of $\mathbf{\Omega}$ with the trial vector **F**. For this reason, we present in the following section a detailed description of this matrix–vector multiplication in our new TDADFT implementation.

Matrix–vector multiplication

For the discussion of the matrix–vector multiplication, **ΩF**, we introduce the trial vector, **VINP**, and the result vector, **VOUT**. For clarity of presentation, we omit the trivial first term of $\mathbf{\Omega}$ in eq. [29] as well as the square roots of the molecular orbital energy differences that multiply the Kohn–Sham matrix elements. In our implementation, the matrix–vector multiplication is organized such that the three-center ERIs are rebuilt on-the-fly each time they are needed. First, we take the initial trial vector, **VINP**, and transform it into an atomic orbital representation. As result, we obtain the matrices $\mathbf{Q}^{\sigma}$ defined by

$$Q^{\sigma}_{\mu\nu} = \sum_{i}^{\mathrm{occ}}\sum_{a}^{\mathrm{uno}} c^{\sigma}_{\mu i}\mathrm{VINP}^{\sigma}_{ia}c^{\sigma}_{\nu a} \quad (31)$$

The superscript σ refers to the α and β spin manifolds. In the next step, the $\mathbf{Q}^{\sigma}$ matrices are multiplied with three-center ERIs yielding the elements of the intermediate **R** vectors.

$$R^{\sigma}_{\overline{k}} = \sum_{\mu,\nu} Q^{\sigma}_{\mu\nu}\langle\mu\nu\|\overline{k}\rangle \quad (32)$$

As already mentioned, the ERIs for this operation are built on-the-fly. The resulting two $\mathbf{R}^{\sigma}_{\overline{k}}$ vectors are of the dimension of the auxiliary function set. These vectors are used to contract the matrices $\mathbf{H}^{\sigma\sigma'}$ defined as

$$\mathbf{H}^{\sigma\sigma'} = \mathbf{G}^{-1} + \mathbf{G}^{-1}\mathbf{f}^{\sigma\sigma'}\mathbf{G}^{-1} \quad (33)$$

in four new vectors, $\boldsymbol{\omega}^{\boldsymbol{\sigma\sigma'}}$, according to

$$\omega^{\sigma\sigma'}_{\overline{k}} = \sum_{\overline{l}} H^{\sigma\sigma'}_{\overline{k}\overline{l}}R^{\sigma'}_{\overline{l}} \quad (34)$$

The four new vectors, $\boldsymbol{\omega}^{\sigma\sigma'}$, have the spin combinations $\alpha\alpha$, $\alpha\beta$, $\beta\alpha$, and $\beta\beta$ and are also of the dimension of the auxiliary function set. These vectors are now multiplied again with the three-center ERIs to form the two matrices, $\mathbf{\Theta}^{\sigma}$, that possess the basis set dimensions:

$$\Theta^{\sigma}_{\mu\nu} = \sum_{\overline{k}} \langle\mu\nu\|\overline{k}\rangle\left(\omega^{\sigma\sigma}_{\overline{k}} + \omega^{\sigma\sigma'}_{\overline{k}}\right) \quad (35)$$

Thus, the ERIs have to be built twice for each matrix–vector multiplication, similar as in a direct self-consistent field (SCF)

Fig. 1. Comparison of the TDADFT photoabsorption spectrum of benzene (black curve) with its experimental counterpart (red curve).

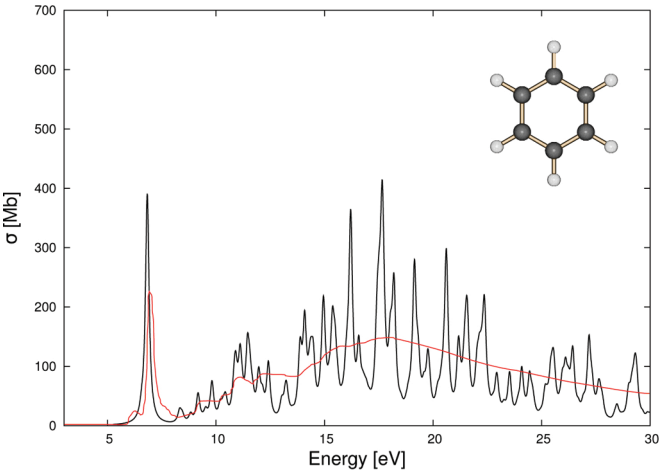

Fig. 2. Comparison of the TDADFT photoabsorption spectrum of naphthalene (black curve) with its experimental counterpart (red curve).

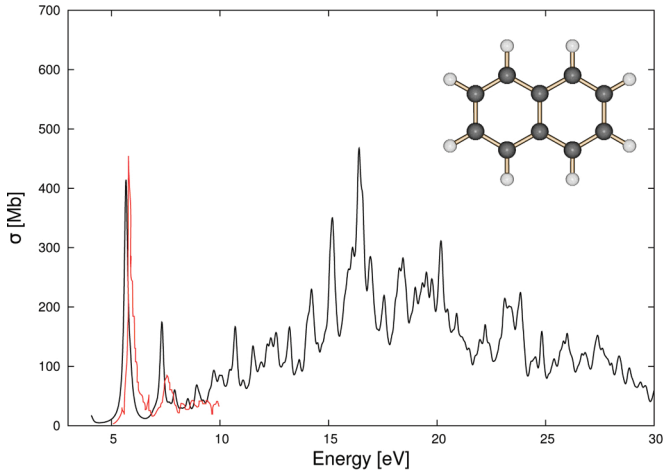

Fig. 3. Comparison of the TDADFT photoabsorption spectrum of 2-methyl-naphthalene (black curve) with its experimental counterpart (red curve).

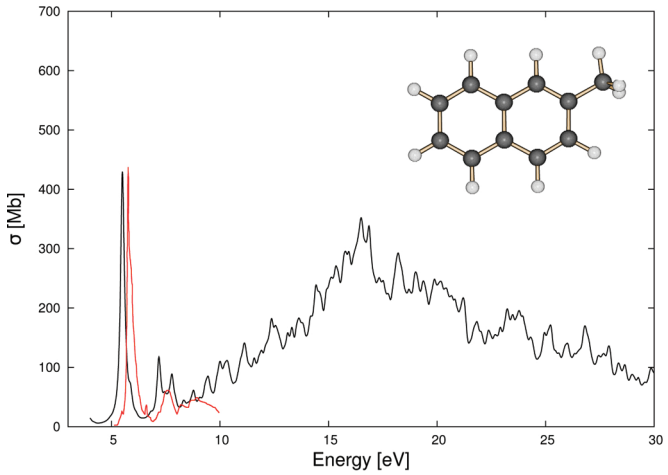

Fig. 4. Comparison of the TDADFT photoabsorption spectrum of anthracene (black curve) with its experimental counterpart (red curve).

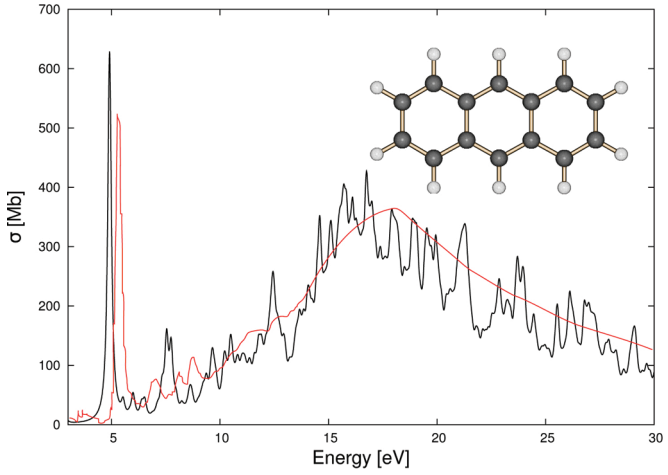

Fig. 5. Dominant MO transitions of the double degenerated $\pi \rightarrow \pi^{\star}$ excitation (top and bottom) at 6.8 eV in benzene that determines the first large peak in its photoabsorption spectrum.

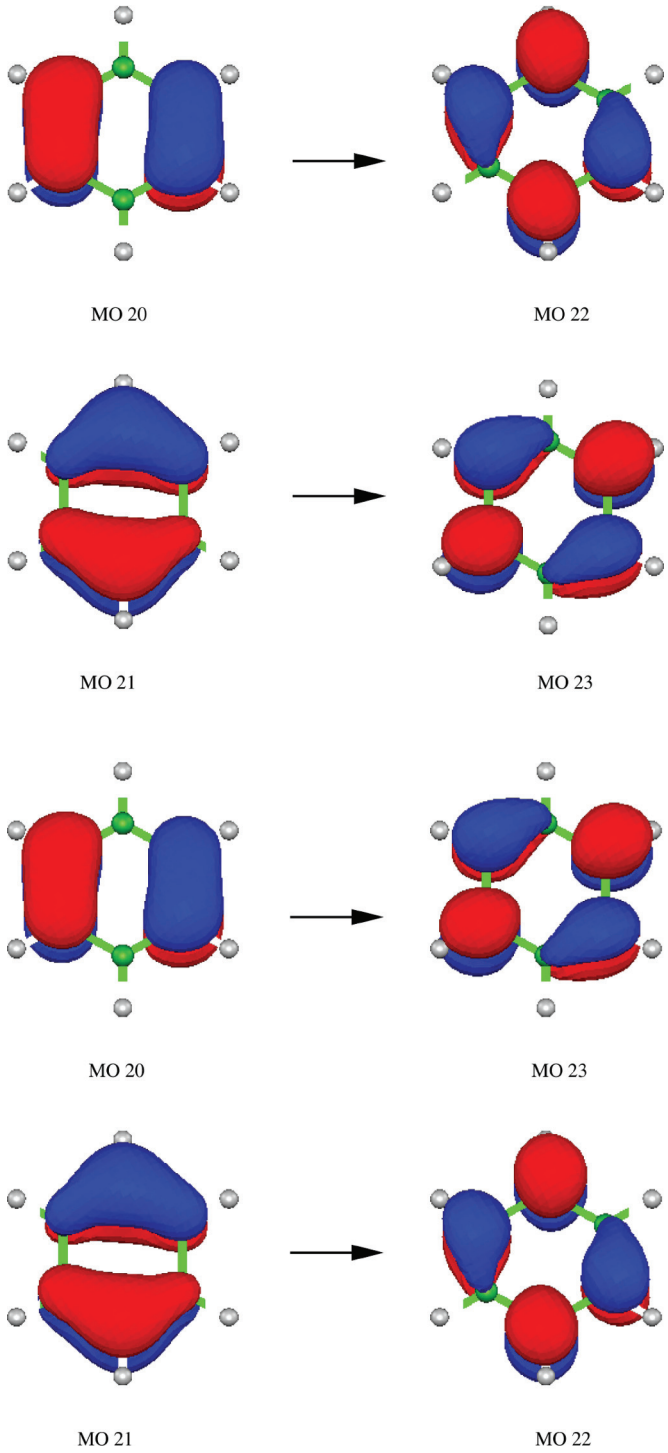

step.[53] In the last step, the two $\mathbf{\Theta}^{\sigma}$ matrices are transformed to a molecular orbital representation to build the result vector, **VOUT**.

$$VOUT^{\sigma}_{ia} = \sum_{\mu,\nu} c^{\sigma}_{\mu i} \Theta^{\sigma}_{\mu\nu} c^{\sigma}_{\nu a} \tag{36}$$

This concludes the matrix–vector multiplication in our implementation of the Davidson algorithm. Thus, no explicit

Fig. 6. Dominant MO transitions of the $\pi \rightarrow \pi^{\star}$ excitation at 5.6 eV in naphthalene that determines the first large peak in its photoabsorption spectrum.

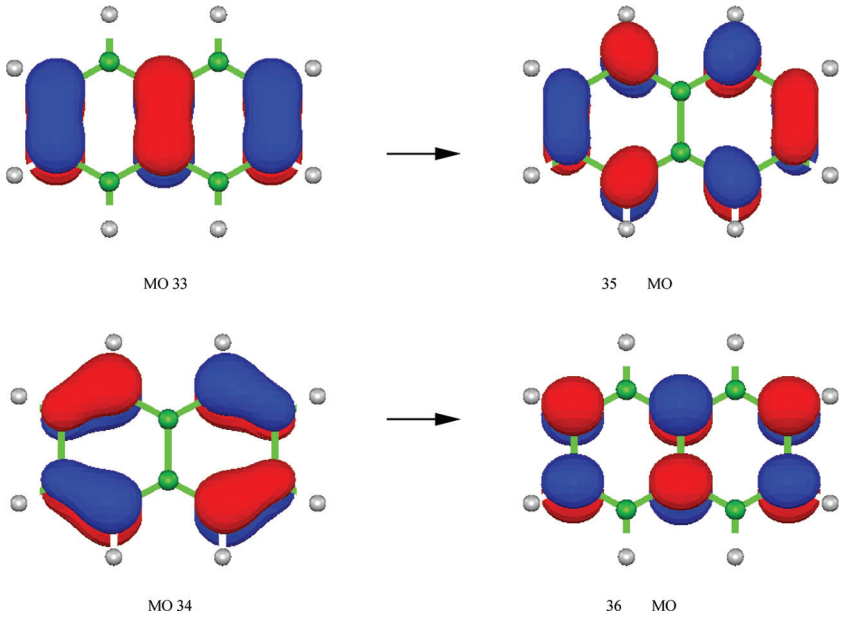

Fig. 7. Dominant MO transitions of the $\pi \rightarrow \pi^{\star}$ excitation at 5.5 eV in 2-methyl-naphthalene that determines the first large peak in its photoabsorption spectrum.

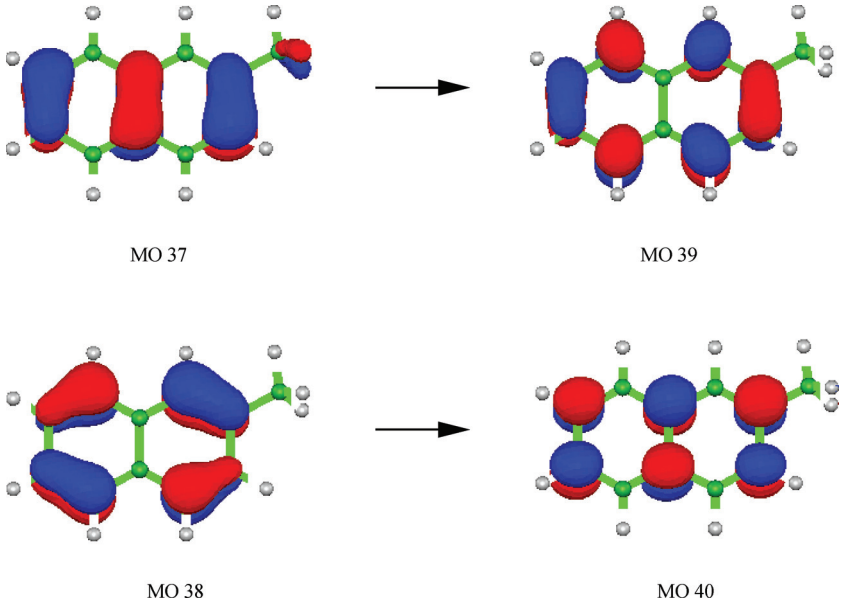

transformation of the three-center ERIs to molecular orbital representation is necessary. Moreover, the memory demand is similar to the direct SCF implementation in deMon2k. For the on-the-fly ERI calculation, efficient parallelized linear scaling integral routines[53] are employed.

Computational methodology

All calculations were carried out with a developer version of the LCGTO-DFT code deMon2k.[38] The Coulomb energy is always calculated by the variational fitting procedure proposed by Dunlap et al.[28] The fitted auxiliary density is used to evaluate the exchange–correlation energy and its derivatives, i.e., potential and kernel.[31,32] In all cases, the exchange–correlation energies and potentials, calculated from the approximated densities, are numerically integrated on an adaptive grid with a 10^{-5} a.u. grid accuracy.[54,55] The same grid is used for the exchange–correlation kernel calculation.

The structures for benzene, naphthalene, 2-methyl-naphthalene, and anthracene were optimized at the LDA level. For this purpose, the Dirac exchange[56] in combination with the VWN[57] correlation functional were employed. The DZVP basis and GEN-A2 auxiliary function sets were used in these optimizations. The molecular structures were optimized in delocalized internal coordinates[58] with a quasi-Newton method.[59] The optimization convergence is based on the analytic gradient and displacement vectors with thresholds of 10^{-4} and 10^{-3} a.u., respectively. Frequency analysis was performed ensuring minimum structures. No symmetry constraints are used, neither in the optimizations nor in the following TDADFT calculations.

Fig. 8. Dominant MO transitions of the $\pi \rightarrow \pi^{\star}$ excitation at 4.9 eV in anthracene that determines the first large peak in its photoabsorption spectrum.

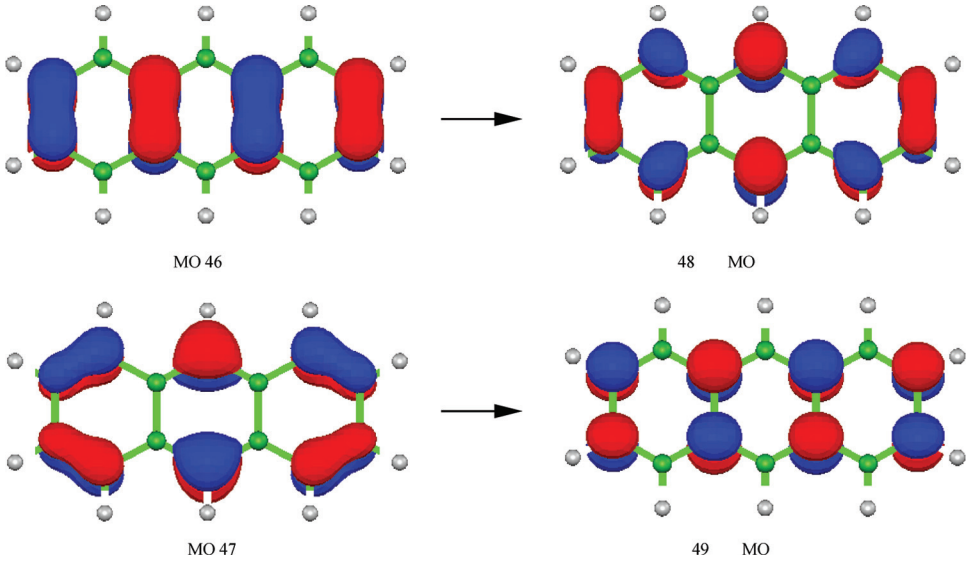

All TDADFT calculations were carried out with the aug-cc-pVTZ[60] basis set in combination with the GEN-A2*[61] auxiliary function set. This auxiliary function set contains *s*, *p*, *d*, *f*, and *g* Hermite Gaussian functions. In Kohn–Sham DFT calculations, the aug-cc-pVTZ basis set yields results close to the basis set limit. In this context, it is worth mentioning that qualitatively similar results can be obtained with considerably smaller basis sets. Thus, the use of the aug-cc-pVTZ basis set in this work is mainly to exclude basis set effects in the validation calculations. In all TDADFT calculations, Dirac exchange[56] in combination with the VWN[57] correlation functional were employed.

To facilitate comparison with experiment we calculated the cross-sections of the discrete TDADFT excitations according to refs. 62–64. These discrete cross-sections were then broadened by a Lorentzian function with a width of 0.4 eV and plotted against the experimental photoabsorption spectra. The cross-sections are given in megabarn (Mb) with 1 Mb being 10^{-22} m^2.

Validation of TDADFT photoabsorption spectra

Figure 1 compares the TDADFT calculated photoabsorption spectrum of benzene (black curve) with its experimental[42] counterpart (red curve). The energy range up to 30 eV was covered by the calculation of the first 1500 singlet–singlet excitations. As Fig. 1 shows, a qualitative good agreement between the calculated and experimental photoabsorption spectrum is obtained. A similar agreement is also found with previously reported real time TDDFT spectra[14,15] of benzene.

Figure 2 compares the calculated TDADFT photoabsorption spectrum of naphthalene (black curve) with its experimental[43] counterpart (red curve). Unfortunately, the experimental spectrum covers only an energy range of up to 10 eV. In this region, the agreement between TDADFT and experiment is satisfying. Despite this reduced experimental energy, we have calculated the photoabsorption spectrum of naphthalene up to 30 eV. This energy range is represented by the first 3500 singlet–singlet excitations in naphthalene. Comparison with corresponding real time TDDFT calculations[14,15] shows agreement similar to benzene.

In Fig. 3, the TDADFT photoabsorption spectrum of 2-methyl-naphthalene (black curve) is compared with its experimental[43] counterpart. Again, the experimental spectrum is only recorded until 10 eV. Nevertheless, we have calculated the spectrum until 30 eV, which is equivalent to the calculation of the first 4500 singlet–singlet excitations. In the available experimental region of the spectrum, a satisfying agreement between experiment and TDADFT is found.

The TDADFT photoabsorption spectrum of anthracene (black curve) is compared with its experimental[42] counterpart (red curve) in Fig. 4. As for the previously discussed systems, a satisfying agreement between TDADFT and experiment is found. A similar good agreement is found for the comparison with real time TDDFT photoabsorption spectra of anthracene.[14,15] The here reported spectrum range of 30 eV is covered by the first 6500 singlet–singlet excitations of anthracene.

By and large, the photoabsorption spectra of the four studied systems are of similar shape. A dominant first peak around or above 5 eV is followed by a characteristic lower intensity structure below 10 eV. After 10 eV, a very broad band is found with a maximum between 15 and 20 eV. The TDADFT calculations show that this broad band arises from a dense group of excitations. The comparison of the first dominant peak at around or above 5 eV in the photoabsorption spectra of benzene, naphthalene, and anthracene shows that this peak moves to lower energies with increasing system size. The comparison of the naphthalene and 2-methyl-naphthalene TDADFT photoabsorption spectra reveals characteristic differences in the region behind the dominant first peak. This can also be seen in the experimental spectra. Whereas in naphthalene a band with a shoulder appears at around 7 eV, in 2-methyl-naphthalene a broad band is observed at a similar energy.

Assignment of selected excitations

As already mentioned, the here employed TDADFT simulation of photoabsorption spectra permits the assignment of individual peaks to underlying orbital transitions. As an illustrative example, we present in Figs. 5–8 the dominant MO excitations for the large first peak in the photoabsorption spectra of benzene, naphthalene, 2-methyl-naphthalene, and anthracene, respectively. As expected, these peaks originate from low-lying $\pi \rightarrow \pi^{\star}$ excitations. In the case of benzene, this excitation is double degenerated due to the degeneracy of the highest occupied MO (HOMO) and lowest unoccupied MO (LUMO). The dominant MO transitions involved in these two excitations are shown in Fig. 5 (top and bottom). All of them are HOMO–LUMO excitations (MO20/21 → MO22/23) as Fig. 5 shows.

In the other three systems, naphthalene, 2-methyl-naphthalene, and anthracene, the first peak of their photoabsorption spectrum can be assigned to one dominant $\pi \rightarrow \pi^{\star}$ excitation that arises from transitions between the two highest occupied MOs (MO33/34, MO37/38, and MO46/47 for naphthalene, 2-methyl-naphthalene, and anthracene, respectively) and the two lowest unoccupied MOs (MO35/36, MO39/40, and MO48/49, respectively) of these systems. Figures 6–8 depict these orbital transitions. From benzene to anthracene, the corresponding excitation energies decrease systematically from 6.8 eV to 4.9 eV as the π system increases. This is the main reason for the shift of the first large peak in the corresponding photoabsorption spectra to lower energies with increasing system size.

Conclusions

The working equations for time-dependent auxiliary density functional theory (TDADFT) are derived by perturbation theory in the framework of ADFT. An efficient implementation on the basis of the Davidson algorithm is presented. Its parallel version is well suited for the calculation of large numbers of excitations. For the validation of this new TDADFT implementation in deMon2k, the photoabsorption spectra of benzene, naphthalene, 2-methyl-naphthalene, and anthracene are calculated up to 30 eV. Comparison with the corresponding experimental spectra demonstrates the accuracy and reliability of TDADFT. In contrast to real time TDDFT simulations of photoabsorption spectra, the here presented TDADFT approach permits the assignment of the underlying excitations. For the discussed polycyclic aromatic hydrocarbons, the low-lying $\pi \rightarrow \pi^{\star}$ excitations have been assigned as an illustrative example.

Acknowledgements

All calculations were performed at the Aitzaloa supercomputing center at the Universidad Autónoma Metropolitana Iztapalapa, Mexico. JCE gratefully acknowledges support from the Consejo Nacional de Ciencia y Technología (CONACYT; postdoctoral fellowship). This work was supported by the CONACYT through the projects CIAM 107310 and CB 179409.

References

(1) Hohenberg, P.; Kohn, W. *Phys. Rev.* **1964**, *136*, B864. doi:10.1103/PhysRev.136.B864.
(2) Kohn, W.; Sham, L. J. *Phys. Rev.* **1965**, *140*, A1133. doi:10.1103/PhysRev.140.A1133.
(3) Chakravarty, S.; Fogel, M. B.; Kohn, W. *Phys. Rev. Lett.* **1979**, *43*, 775. doi:10.1103/PhysRevLett.43.775.
(4) Bartolotti, L. J. *Phys. Rev. A* **1981**, *24*, 1661. doi:10.1103/PhysRevA.24.1661.
(5) Bartolotti, L. J. *Phys. Rev. A* **1982**, *26*, 2243. doi:10.1103/PhysRevA.26.2243.
(6) Deb, B. M.; Gosh, S. K. *J. Chem. Phys.* **1982**, *77*, 342. doi:10.1063/1.443611.
(7) Gosh, S. K.; Deb, B. M. *Chem. Phys.* **1982**, *71*, 295. doi:10.1016/0301-0104(82)87030-4.
(8) Runge, E.; Gross, E. K. U. *Phys. Rev. Lett.* **1984**, *52*, 997. doi:10.1103/PhysRevLett.52.997.
(9) Mearns, D.; Kohn, W. *Phys. Rev. A* **1987**, *35*, 4796. doi:10.1103/PhysRevA.35.4796.
(10) Gross, E. K. U.; Kohn, W. *Adv. Quantum Chem.* **1990**, *21*, 255. doi:10.1016/S0065-3276(08)60600-0.
(11) Marques, M. A. L.; Ullrich, C. A.; Nogueira, F.; Rubio, A.; Burke, K.; Gross, E. K. U. *Time-Dependent Density Functional Theory, Lecture Notes in Physics*; Vol. 706; Springer-Verlag, Berlin, 2006.
(12) Marques, M. A. L.; Maitra, N. T.; Nogueira, F. M. S.; Gross, E. K. U.; Rubio, A. *Fundamentals of Time-Dependent Density Functional Theory, Lecture Notes in Physics*; Vol. 837; Springer-Verlag, Berlin, 2012.
(13) Yabana, K.; Bertsch, G. F. *Int. J. Quantum Chem.* **1999**, *75*, 55. doi:10.1002/(SICI)1097-461X(1999)75:1<55::AID-QUA6>3.0.CO;2-K, 10.1002/(SICI)1097-461X(1999)75:1<55::AID-QUA6>3.3.CO;2-B.
(14) Malloci, G.; Mulas, G.; Cappellini, G.; Joblin, C. *Chem. Phys.* **2007**, *340*, 43. doi:10.1016/j.chemphys.2007.07.046.
(15) Cappellini, G.; Malloci, G.; Mulas, G. *Superlattices and Microstructures* **2009**, *46*, 14. doi:10.1016/j.spmi.2008.12.019.
(16) Koponen, L.; Puska, M. J.; Nieminen, R. M. *J. Chem. Phys.* **2008**, *128*, 154307. doi:10.1063/1.2907742.
(17) Kawashita, Y.; Yabana, K.; Noda, M.; Nobusada, K.; Nakatsukasa, T. *J. Mol. Struct. (THEOCHEM)* **2009**, *914*, 130. doi:10.1016/j.theochem.2009.04.022.
(18) Lopez, X.; Marques, M. A.; astro, A.; Rubio, A. *J. Am. Chem. Soc.* **2005**, *127*, 12329. doi:10.1021/ja050935l.
(19) Flores-Moreno, R.; Köster, A. M. *J. Chem. Phys.* **2008**, *128*, 134105. doi:10.1063/1.2842103.
(20) Flores-Moreno, R.; Melin, J.; Ortiz, J. V.; Merino, G. *J. Chem. Phys.* **2008**, *129*, 224105. doi:10.1063/1.3036926.
(21) Flores-Moreno, R. *J. Chem. Theory Comput.* **2010**, *6*, 48. doi:10.1021/ct9002527.
(22) Shedge, S. V.; Carmona-Espíndola, J.; Pal, S.; Köster, A. M. *J. Phys. Chem. A* **2010**, *114*, 2357. doi:10.1021/jp909966f.
(23) Shedge, S. V.; Pal, S.; Köster, A. M. *Chem. Phys. Lett.* **2011**, *510*, 185. doi:10.1016/j.cplett.2011.05.032.
(24) Zuñiga-Gutierrez, B.; Geudtner, G.; Köster, A. M. *J. Chem. Phys.* **2011**, *134*, 124108. doi:10.1063/1.3567493.
(25) Zuñiga-Gutierrez, B.; Geudtner, G.; Köster, A. M. *J. Chem. Phys.* **2012**, *137*, 094113. doi:10.1063/1.4749243.
(26) Köster, A. M.; Reveles, J. U.; del Campo, J. M. *J. Chem. Phys.* **2004**, *121*, 3417. doi:10.1063/1.1771638.
(27) Calaminici, P.; Dominguez-Soria, V. D.; Flores-Moreno, R.; Gamboa, G. U.; Geudtner, G.; Goursot, A.; Salahub, D. R.; Köster, A. M. *Auxiliary Density Functional Theory: From Molecules to Nanostructures in Handbook of Computational Chemistry*; Leszczynski, J., Ed.; Springer-Verlag, Berlin, 2011.
(28) Dunlap, B. I.; Connolly, J. W. D.; Sabin, J. R. *J. Chem. Phys.* **1979**, *71*, 4993.
(29) Mintmire, J. W.; Dunlap, B. I. *Phys. Rev. A* **1982**, *25*, 88. doi:10.1103/PhysRevA.25.88.
(30) Dunlap, B. I.; Rösch, N.; Trickey, S. B. *Mol. Phys.* **2010**, *108*, 3167. doi:10.1080/00268976.2010.518982.
(31) Carmona-Espíndola, J.; Flores-Moreno, R.; Köster, A. M. *J. Chem. Phys.* **2010**, *133*, 084102. doi:10.1063/1.3478551.
(32) Carmona-Espíndola, J.; Flores-Moreno, R.; Köster, A. M. *Int. J. Quantum Chem.* **2012**, *112*, 3461. doi:10.1002/qua.24082.
(33) Calaminici, P.; Carmona-Espíndola, J.; Geudtner, G.; Köster, A. M. *Int. J. Quantum Chem.* **2012**, *112*, 3252. doi:10.1002/qua.24176.
(34) Shedge, S. V.; Pal, S.; Köster, A. M. *Chem. Phys. Lett.* **2012**, *552*, 146. doi:10.1016/j.cplett.2012.09.045.
(35) Casida, M. E. In *Recent Advances in Density Functional Methods I*; Chong, D. P., Ed.;World Scientific, Singapore, 1995; pp. 155.
(36) Jamorski, C.; Casida, M. E.; Salahub, D. R. *J. Chem. Phys.* **1996**, *104*, 5134.
(37) Ipatov, A.; Fouqueau, A.; Perez del Valle, C.; Cordova, F.; Casida, M. E.; Köster, A. M.; Vela, A.; Jamorski, C. J. *J. Mol. Struct. (THEOCHEM)* **2006**, *179*, 762.
(38) Köster, A. M.; Geudtner, G.; Calaminici, P.; Casida, M. E.; Dominguez-Soria, V. D.; Flores-Moreno, R.; Gamboa, G. U.; Goursot, A.; Heine, T.; Ipatov, A.; Janetzko, F.; del Campo, J. M.; Reveles, J. U.; Vela, A.; Zuniga-Gutierrez, B.; Salahub, D. R. *deMon2k*, Version 3; The deMon Developers, Cinvestav, Mexico-City, 2011.
(39) Geudtner, G.; Calaminici, P.; Carmona-Espíndola, J.; del Campo, J. M.; Dominguez-Soria, V. D.; Flores-Moreno, R.; Gamboa, G. U.; Goursot, A.; Köster, A. M.; Reveles, J. U.; Mineva, T.; Vasquez-Perez, J. M.; Vela, A.; Zuñiga-Gutierrez, B.; Salahub, D. R. *Wiley Interdisciplinary Reviews: Computational Molecular Science* **2012**, *2*, 548. doi:10.1002/wcms.98.
(40) Davidson, E. R. *J. Comp. Phys.* **1975**, *17*, 87.
(41) Cisneros, G.; Berrondo, M.; Bunge, C. F. *Comp. Chem.* **1986**, *10*, 281. doi:10.1016/0097-8485(86)85016-1.
(42) Joblin, C.; Léger, A.; Martin, P. *Astrophys. J.* **1992**, *393*, L79. doi:10.1086/186456.
(43) Gingell, J. M. *Faraday Discuss.* **1998**, *109*, 361. doi:10.1039/FD109361.
(44) Hahn, J. H.; Zenobi, R.; Bada, J. L.; Zare, R. N. *Science* **1998**, *239*, 1523. doi:10.1126/science.239.4847.1523.
(45) Clemett, S. J.; Maechling, C. R.; Zare, R. N.; Swan, P. D.; Walker, R. M. *Science* **1993**, *262*, 721. doi:10.1126/science.262.5134.721.
(46) Tielens, A. G. G. M. *The Physics and Chemistry of the Interstellar Medium*; Cambridge University Press, Cambridge, 2005.
(47) van Leeuwen, R. *Phys. Rev. Lett.* **1999**, *82*, 3863. doi:10.1103/PhysRevLett.82.3863.
(48) Carmona Espíndola, J. *Time-Dependent Auxiliary Density Perturbation Theory: Method, Implementation and Applications*; Ph.D. thesis, Cinvestav, México, 2012.
(49) Čížek, J.; Paldus, J. *J. Chem. Phys.* **1967**, *47*, 3976. doi:10.1063/1.1701562.
(50) Petersilka, M.; Gross, E. K. U. *Int. J. Quantum Chem. Symp.* **1996**, *30*, 181.
(51) Bauernschmitt, R.; Ahlrichs, R. *Chem. Phys. Lett.* **1996**, *256*, 454. doi:10.1016/0009-2614(96)00440-X.
(52) van Gisbergen, S. J. A.; Snijders, J. G.; Baerends, E. J. *Comp. Phys. Comm.* **1999**, *118*, 119. doi:10.1016/S0010-4655(99)00187-3.
(53) Geudtner, G.; Janetzko, F.; Köster, A. M.; Vela, A.; Calaminici, P. *J. Comp. Chem.* **2006**, *27*, 483. doi:10.1002/jcc.20361.
(54) Krack, M.; Köster, A. M. *J. Chem. Phys.* **1998**, *108*, 3226. doi:10.1063/1.475719.
(55) Köster, A. M.; R.; Flores-Moreno, R.; Reveles, J. U. *J. Chem. Phys.* **2004**, *121*, 681. doi:10.1063/1.1759323.
(56) Dirac, P. A. M. *Proc. Cambr. Phil. Soc.* **1930**, *26*, 376. doi:10.1017/S0305004100016108.

(57) Vosko, S. H.; Wilk, L.; Nusair, M. *Can. J. Phys.* **1980**, *58* (8), 1200. doi:10.1139/p80-159.
(58) Reveles, J. U.; Köster, A. M. *J. Comput. Chem.* **2004**, *25*, 1109. doi:10.1002/jcc.20034.
(59) del Campo, J. M.; Köster, A. M. *J. Chem. Phys.* **2008**, *129*, 024107. doi:10.1063/1.2950083.
(60) Dunning, T. H. *J. Chem. Phys.* **1989**, *90*, 1007. doi:10.1063/1.456153.
(61) Calaminici, P.; Janetzko, F.; Köster, A. M.; Mejia-Olvera, R.; Zuniga-Gutierrez, B. *J. Chem. Phys.* **2007**, *126*, 044108. doi:10.1063/1.2431643.
(62) Hilborn, R. C. *Am. J. Phys.* **1982**, *50*, 982. doi:10.1119/1.12937.
(63) Atkins, P. W. *Physikalische Chemie*; VCH, Weinheim, 1987; pp. 477.
(64) Natarajan, B.; Genovese, L.; Casida, M. E.; Deutsch, T.; Burchak, O. N.; Philouze, C.; Balakirev, M. Y. *Chem. Phys.* **2012**, *402*, 29. doi:10.1016/j.chemphys.2012.03.024.